Biotechnology Journal
www.biotechnology-journal.com

Plasmonic Biosensor Controlled by DNAzyme for On-Site Genetic Detection of Pathogens

*Woogi Lee and Byeong Hee Hwang**

On-site predetection of pathogens could significantly decrease of a disease outbreak or national loss in most of the countries. However, conventional detection techniques are limited in use for on-site detection due to the necessity of specialized skill or equipment. Therefore, it is necessary to develop a new technique that can predetect pathogens in the field without special skills or equipment. Here, a DNAzyme strategy to control a plasmonic biosensor for rapid and simple visual detection of *Salmonella choleraesuis* is adopted. Multicomponent DNAzyme formed by target addition can cleave the linker effectively at 50 °C. Linker cleavage induces dispersion of two DNA-immobilized gold nanoparticles and color change. Under optimized assay conditions, the target could be detected via visual discrimination sensitively and specifically. Moreover, the biosensor shows the possibility of practical use with contaminants and a 16S rRNA real target. As a result, the proposed plasmonic biosensor can visually detect *S. choleraesuis* without unstable enzymes, a specialized technique, or equipment. Therefore, these advantages could allow that this biosensor would be used for on-site predetection to lower the risk of transmission of infectious diseases.

1. Introduction

Infectious diseases cause lots of patients and national loss annually in most countries. Since some pathogens have strong infectivity, early diagnosis and isolation of infected patients are essential to prevent the spread of infectious diseases. However, since the diagnosis is made only at a medical institution, early diagnosis of pathogenic diseases is very difficult due to limited accessibility to a medical institution in many countries, including developing countries.[1,2] Furthermore, the needs of skilled personnel and expensive equipment for diagnostic techniques make the predetection of pathogens difficult.[3] Therefore, it is necessary to develop a new technique that can predetect pathogens in the field without special skills or equipment.[4]

Currently, the conventional detection method is based on a culture of bacterial pathogens, but it takes a long procedural time (up to several days) and has limitations in identification of specific species.[5–7] Therefore, relatively rapid, sensitive, and specific methods are widely developed, including enzyme-linked immunosorbent assays (ELISA) and polymerase chain reaction (PCR).[8,9] However, both ELISA and PCR require skilled personnel, expensive reagents, and equipped laboratory limited in resource-poor countries.[10]

Therefore, unlike traditional laboratory-based techniques, relatively simple techniques have been developed for detecting pathogens in a resource-poor environment.[11,12] Microfluidic electrochemical loop-mediated isothermal amplification could detect pathogenic DNAs rapidly, sensitively, and quantitatively.[11] The litmus test was adopted for bacterial detection by coupling bacteria-specific RNA-cleaving DNAzyme and urease on magnetic beads.[12] These technologies were able to detect pathogens simpler than existing technologies. However, it still needs complicated skills or proteins that are difficult to store or use.

Here, we adopted a DNAzyme strategy to develop a plasmonic biosensor for rapid and simple visual detection of *Salmonella choleraesuis*. Enzymatic cleavage of multicomponent DNAzymes induced the colorimetric signal of gold nanoparticles (GNPs) using the previous literature.[13] GNPs are widely used in the detection filed because it provides visible colorimetric results.[14–17] Synthesized GNPs were immobilized with two different thiolated DNA of Imm1 and Imm2 to make GNP-1 and GNP-2, respectively. After the confirmation of multicomponent DNAzyme formation, colorimetric change of plasmonic biosensor was observed through target cleavage using DNAzyme. Under the optimization of DNAzyme reaction conditions, the sensitivity and specificity of the biosensor were determined. The practical usability was tested using detections in contaminants, and with16S rRNA real target.

W. Lee, Prof. B. H. Hwang
Department of Bioengineering and Nano-bioengineering
Incheon National University
Incheon 22012, Korea
E-mail: bhwang@inu.ac.kr
Prof. B. H. Hwang
Division of Bioengineering
Incheon National University
Incheon 22012, Korea

The ORCID identification number(s) for the author(s) of this article can be found under https://doi.org/10.1002/biot.201900329

DOI: 10.1002/biot.201900329

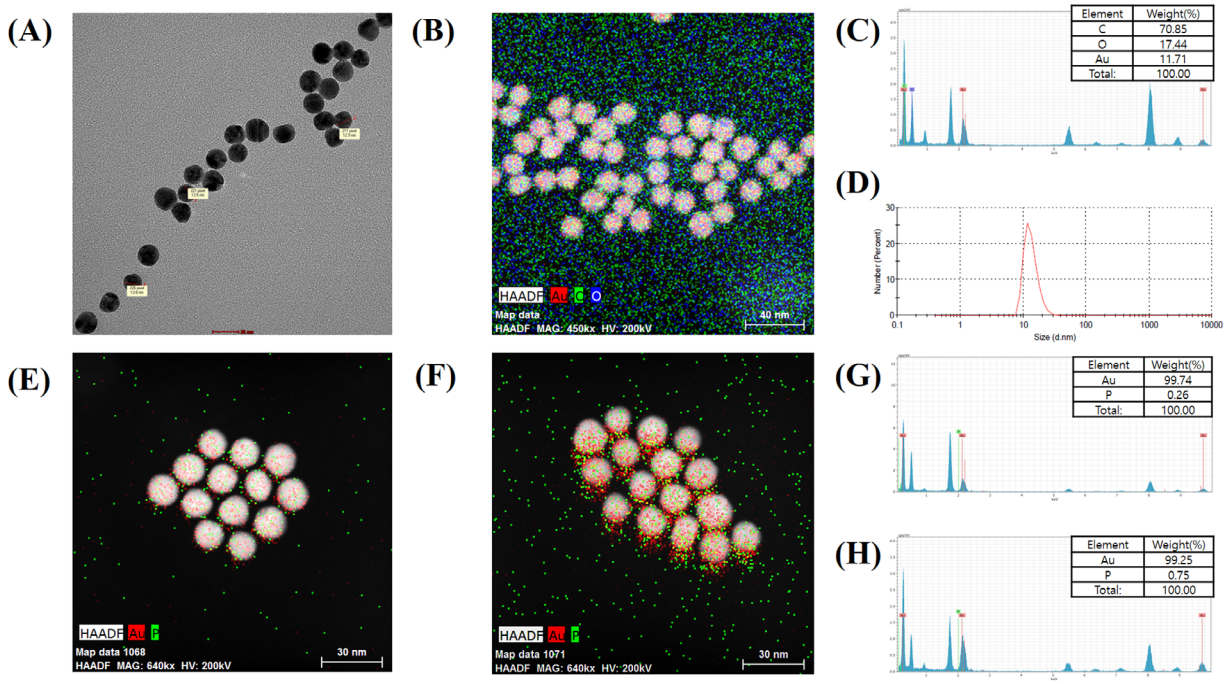

Figure 1. Characterization of GNPs and immobilization of thiolated DNA on GNPs: A) TEM image of synthesized GNPs (245 000×). B) EDS mapping image of synthesized AuNPs. The red dot on the measured nanoparticle was verified to GNPs; C) spectra of AuNPs analyzed by EDS, and D) size distribution of AuNPs measured by DLS. E) EDS spectra of Imm1-immobilized GNPs, and F) EDS spectra of Imm2-immobilized GNPs. Red spots indicated the distribution of gold and green spots indicated the distribution of phosphate. G) EDS element mapping image of Imm1-immobilized GNPs, H) EDS element mapping image of Imm2-immobilized GNPs.

2. Results

2.1. Characterization of GNPs w/o and w/ Thiolated DNA

Physical properties of fabricated GNPs were characterized by transmission electron microscope (TEM), dynamic light scattering (DLS), scanning electron microscopy (SEM), and energy dispersive spectrometry (EDS). First, the TEM image represented the well-dispersed uniform size and spherical shape with a regular size of average 13.5 nm (**Figure 1**A; Figure S1, Supporting Information). EDS mapping showed that the nanoparticles composed of gold with red dots (Figure 1B). EDS spectra proved that nanoparticles were made of gold with a gold peak of 11.71 wt% (Figure 1C). Also, DLS analysis indicated that the average size of GNPs by DLS was 13.45 nm with PDI 0.103, and the size distribution was unimodal (Figure 1D). The size of GNPs was coincided by both TEM and DLS analyses. Zeta potential of synthesized GNPs was −11.7 mV measured by DLS (Figure S2A, Supporting Information). As a result, GNPs were successfully fabricated with uniform size, shape, and relatively negative charge.

The conjugation of thiolated DNA to GNPs was confirmed using SEM, TEM, EDS, and zeta potential. The element mapping and peaks of GNPs conjugated by Imm1 and Imm2 were observed by EDS analysis of TEM, respectively (Figure 1E–H). EDS element mapping showed red spots (gold) and green spots (phosphate) on the nanoparticles (Figure 1E,F). Gold and phosphate peaks were observed using EDS analysis of TEM and SEM (Figures 1G,H; Figure S3A,B, Supporting Information). The well-dispersed GNPs were observed with uniform size and spherical shape in both cases (Figure S3D,E, Supporting Information). Zeta potentials of Imm1-immobilized and Imm2-immobilized GNPs were −17.7 and −13.4 mV, respectively (Figure S2B,C, Supporting Information). Moreover, the aggregation of GNPs conjugated by thiolated DNA was observed using SEM and EDS analysis. After the linker addition, the aggregation of GNPs with Imm1 and Imm2 was observed by the SEM image (Figure S3F, Supporting Information). Also, phosphate and gold peaks of aggregated GNPs were observed by EDS (Figure S3C, Supporting Information). The relative weight proportion of phosphate in aggregated GNPs increased.

2.2. Confirmation of DNAzyme Reaction and Plasmonic DNAzyme Assay

Operations of DNAzyme reaction and plasmonic DNAzyme assay were confirmed through experiments. The operation of the DNAzyme reaction was demonstrated by agarose gel electrophoresis (Figure S4, Supporting Information). The bands of MNAzyme A, MNAzyme B, and linker were observed in the fourth lane without the target. In the fifth lane, when the target addition, the upper band was considered as a DNAzyme complex. The DNAzyme complex composed of MNAzyme A, MNAzyme B, linker, and target. The lower band was considered as a cleaved linker because the size of the cleaved linker is shorter than that of the linker or other MNAzymes. Therefore, the

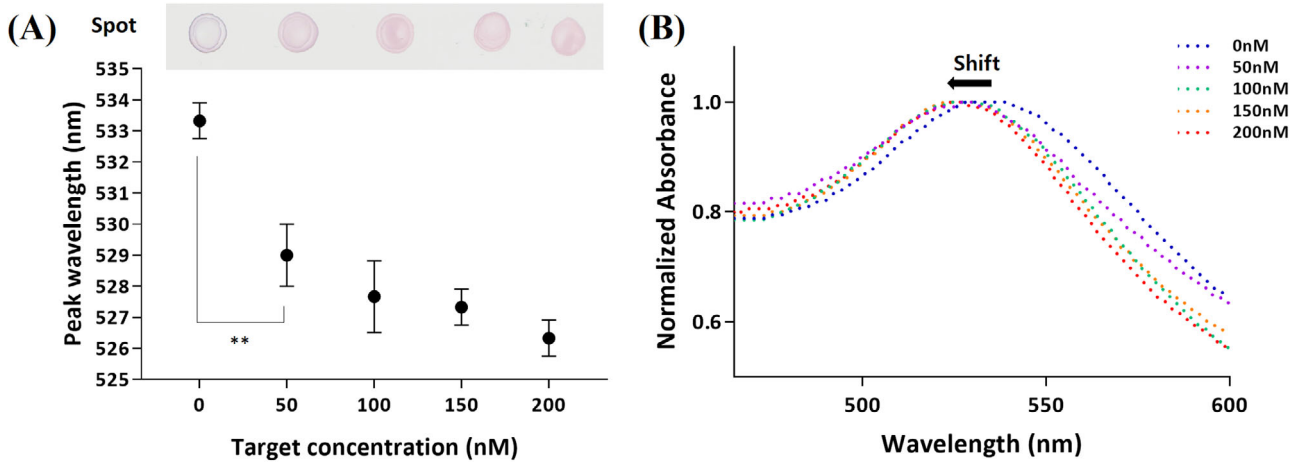

Figure 2. The sensitivity of the colorimetric biosensor. A) Top: spot image of 0–200 nM target on nitrocellulose membrane. Image was adjusted for contrast and brightness. Bottom: The shift of peak absorbance wavelength was observed for the change target concentration from 0 to 200 nM. The data represented mean ± standard deviation. Experiments were repeated four times independently. The *p*-value was calculated using *t*-test. ** means $p < 0.01$. B) The maximum wavelength in normalized absorbance spectra was shifted based on the target concentration change from 0 to 200 nM.

presence of a cleaved linker band has proved the regular operation of DNAzyme.

The operation of the plasmonic DNAzyme assay was demonstrated by colorimetric change and shift of peak wavelength (Figure S5, Supporting Information). The color of GNPs without target was indigo blue, and the color was changed to pale pink gradually as target concentration increased (Figure S5A, Supporting Information). Moreover, the peak wavelength of GNPs without target was 527 nm, and the peak wavelength was shifted to 523 nm gradually as target concentration increased (Figure S5B, Supporting Information).

2.3. Optimization of Reaction Conditions

Temperature, time, and linker concentration were optimized through experiments for the best sensitivity. For the optimization of temperature, the cleaved linker was observed by agarose gel electrophoresis (Figure S6A, Supporting Information), and the change of peak wavelength was observed by a UV microplate reader (Figure S7, Supporting Information). The band longer than the linker was considered as a DNAzyme complex in an upper white rectangle, and the band shorter than the linker was considered as the cleaved linker in a lower white rectangle. The brightest band of the cleaved linker was observed at 50 °C. Besides, a dramatic shift of peak wavelength in the absorbance spectrum at 50 °C was observed compared to that at 65 °C (Figure S7, Supporting Information). Therefore, 50 °C was chosen for the reaction temperature of the following experiments.

For the optimization of reaction time, the cleaved linker was observed by agarose gel electrophoresis (Figure S6B, Supporting Information). The more extended band and shorter band than the linker was considered as the DNAzyme complex and the cleaved linker, respectively. The band intensity of the cleaved linker increased dramatically until 1 h. After 1 h, the band intensity does not show significant change. Therefore, 1 h was chosen for the adequate reaction time of the following experiments.

The linker concentration was optimized by a shift of peak wavelength (Figure S8, Supporting Information). The aggregated particles showed around 535 nm of peak wavelength. As the target concentration increased, the peak wavelength decreased to around 525 nm. A shift of peak wavelength was observed at 300 and 400 nM among 200–700 nM linker concentrations (Figure S8B,C, Supporting Information). Specifically, the peak wavelength at 300 nM linker concentration diminished gradually and linearly and from 0 to 150 nM of target concentration (Figure S8B, Supporting Information). Peak wavelength at 400 nM linker concentration decreased steeply from 0 to 100 nM of target concentration (Figure S8C, Supporting Information). For the best sensitivity, the following experiments were performed at a 400 nM linker concentration.

2.4. Sensitivity and Specificity of Plasmonic DNAzyme Assay

The sensitivity of the plasmonic DNAzyme assay was determined by a shift of peak wavelength (**Figure 2**). Peak wavelength decreased steeply from 0 to 50 nM of the target concentration (Figure 2A). Then, the peak wavelength decreased gradually from 50 to 200 nM of the target concentration. The peak wavelength of 50 nM target concentration was significantly different from the peak wavelength of 0 nM target concentration. *p*-value was 0.00289 by the *t*-test from three independent repeats. Moreover, the normalized absorbance spectrum clear showed wavelength shift to shorter value (Figure 2B). The limit of detection was determined as 50 nM because of statistically significant difference and optically distinguishable color.

The specificity of the plasmonic DNAzyme assay was evaluated using mismatched targets (**Figure 3**). M1, M2, and M3 were designed with one, two, and three adjacent mismatches. All mismatched targets showed no significant color change in spot pictures (Figure 3). Moreover, the maximal difference of peak wavelength was 3 nm, which could not be discriminated against with colorimetric change. Therefore, the specificity of the

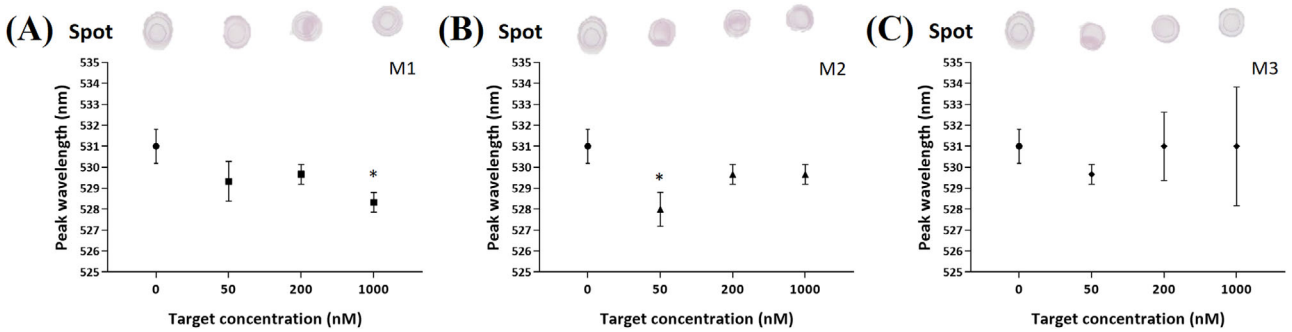

Figure 3. The specificity of the colorimetric biosensor. M1, M2, and M3 were designed as having one, two, and three mismatches, respectively. Three graphs represented the result using A) M1, B) M2, and C) M3 targets, respectively. Top, spot image on nitrocellulose membrane; bottom, the shift of peak absorbance wavelength of 0–1000 nM target concentration. The spot and error bars indicated the average and standard deviations. Experiments were repeated three times independently. The *p*-value was calculated using *t*-test. * means $p < 0.05$.

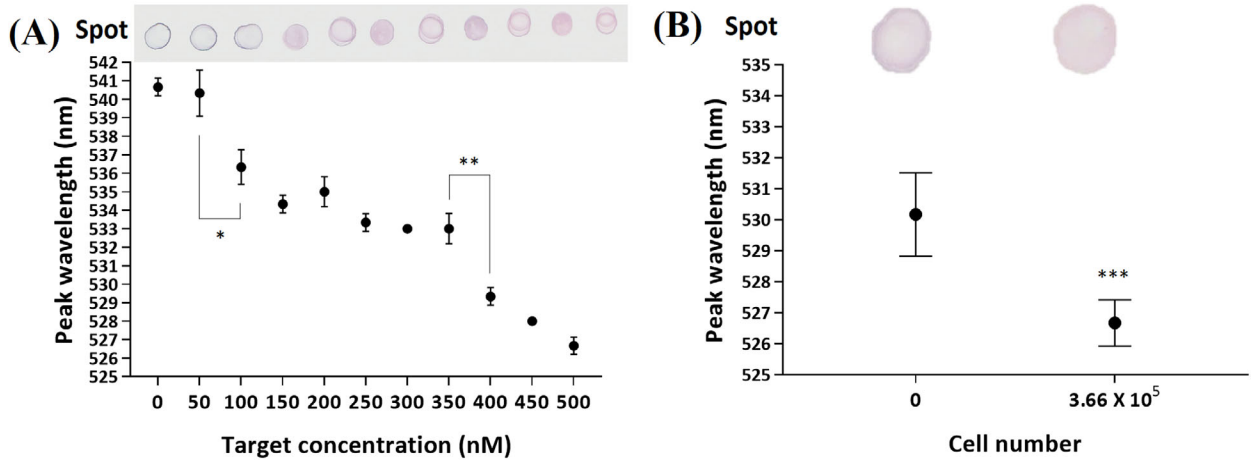

Figure 4. Practical usability test using contaminants and a 16S rRNA real target. A) Colorimetric detection with LB broth. Top, spot image on nitrocellulose membrane; bottom, the shift of peak absorbance wavelength of 0–500 nM target concentration. Experiments were repeated three times independently. B) Colorimetric detection using 16S rRNA real target. Top, spot image on nitrocellulose membrane; bottom, the shift of peak absorbance wavelength of purified total RNA equivalent to 3.66×10^5 cells. The spots and error bars indicated the average and standard deviations in both graphs. Experiments were repeated five times independently. The *p*-value was calculated using *t*-test. *, **, and *** mean $p < 0.05$, 0.01, and 0.001, respectively.

proposed biosensor could discriminate one base mismatch of a target.

2.5. Practical Usability Test of Plasmonic DNAzyme Assay

Detections with contaminants and a real 16S rRNA target were checked using plasmonic DNAzyme assay (**Figure 4**). Because Luria–Bertani media as contaminants had brown color and salt, it could affect the detection of the colorimetric biosensor. The visual spot color was changed at 150 nm of target concentration (Figure 4A). On the other hand, the change in peak wavelength showed a statistically significant difference at 100 nm. Moreover, detection with the real target was confirmed using purified 16S rRNA (Figure 4B). Total RNA was extracted from *S. choleraesuis*. 16S rRNA target equivalent to 3.66×10^5 cells showed distinguishable color change of spots and statistically significant difference. Therefore, the proposed colorimetric biosensor could detect the target sequence in the presence of contaminants and real 16S rRNA target.

3. Discussion

This biosensor could generate the colorimetric signal of the plasmonic field influenced by aggregation of GNPs through DNA linking and dispersion of GNPs by DNAzyme for on-site genetic detection of a pathogen (**Figure 5**). First, if the target sequence existed in the sample, target sequences bound to complementary sequences in the MNAzyme A and B strands, resulting in MNAzyme activation. The Linker sequences were hybridized to the other side of the MNAzymes. The activated MNAzymes with the coenzyme Mg^{2+} cleaved between rG and rU of the Linker sequence. On the surface of GNPs, Imm1 and Imm2 sequences were separately immobilized using thiol bonds. Linker was designed complementarily to the Imm1 and Imm2 sequences. It hybridized with the Imm1 and Imm2 sequences and made an aggregation of GNPs. However, the cleaved Linker did not make an aggregation of GNPs close because each cleaved part is separately combined with Imm1 and Imm2 sequences. In results, the GNPs remain dispersed. In summary, if there is no target, the genuine Linker allowed the GNPs to be aggregated, and the solution

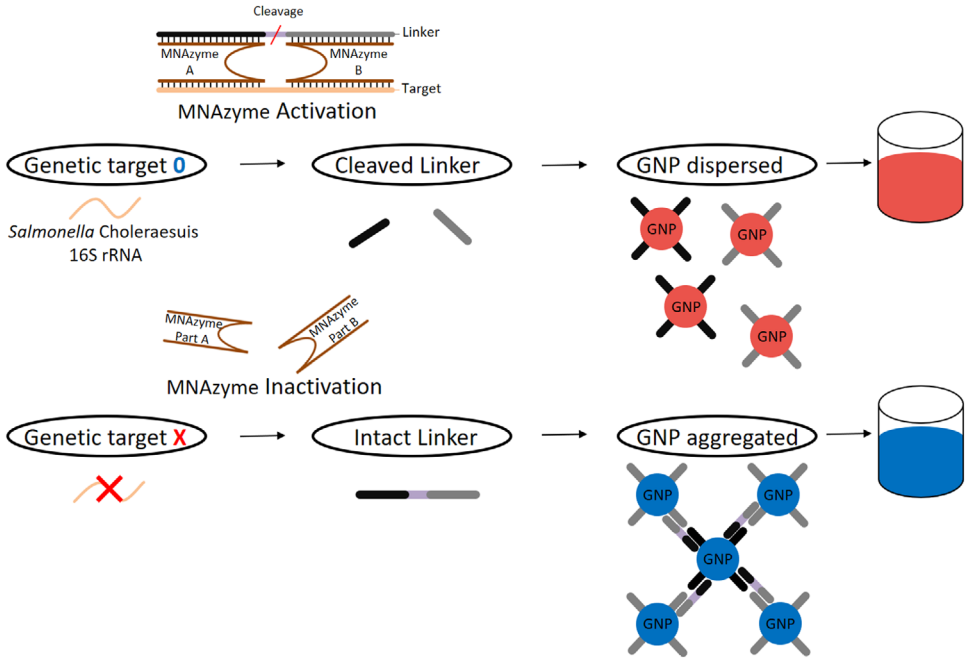

Figure 5. The schematic figure for the overall reaction of the plasmonic biosensor. With a target, activated MNAzyme cleaved the linker, and dispersed Imm1- and Imm2-immobilized GNPs represented red color. Without a target, inactivated MNAzyme could not cleave the linker and aggregated Imm1- and Imm2-immobilized GNPs represented a dark blue color.

became purple or blue. On the other hand, in the presence of target sequences, the Linker sequences were cleaved by the activation of MNAzyme. Then, the solution became red due to the dispersion of the GNPs. GNP-1 and GNP-2 were functionalized with two different thiolated DNA of Imm1 and Imm2, respectively.[18] The linker DNA can form an aggregation of GNP-1 and GNP-2 through hybridization with Imm1 and Imm2 (Figure S3F, Supporting Information). The aggregation of GNPs causes the coupling of a plasmonic field, which affects the shift of maximum absorbance to longer wavelength.[19,20] The color of the solution changes from pale red to dark indigo (Figure S5A, Supporting Information). Moreover, assembled DNAzymes specific to target could cleave two RNA nucleotides of the linker DNA.[21,22] This biosensor chose MNAzyme because it has the highest DNAzyme rate.[23] GNPs dispersed by DNAzymes decoupled the plasmonic field of GNPs, the color of the solution return to pale red. Therefore, the target DNA sequence could be detected using the color change of biosensor.

First, fabricated GNPs had a uniform average diameter of 13.45 nm with unimodal peak analyzed by TEM, SEM, EDS, and DLS. Then, immobilization of Imm1 and Imm2 were checked using the characteristic phosphate spots and peaks of GNP-1, GNP-2, their aggregation in each EDS graph (Figure 1E–H; Figure S2A,B, Supporting Information), and decrease of zeta potential (Figure S2, Supporting Information). Also, DNA immobilization could be supported by the SEM image of aggregated GNPs by linker addition also supported the DNA immobilization (Figure S3F, Supporting Information) and the dark indigo color and shift of absorbance peak to longer wavelength (Figure 3A,B, Supporting Information). The activity of the assembled DNAzyme was checked (Figure S4, Supporting Information). Then, the temperature and time of the proposed biosensor were optimized (Figure S5, Supporting Information). The temperature of 50 °C was chosen due to the brightest band of the cleaved linker (Figure S6A, Supporting Information). This result shows almost a similar tendency as the reference.[13] Time of 1 h was chosen due to the saturated band of the cleaved linker and rapid detection (Figure S6B, Supporting Information).

DNAzyme activity by target addition changed to the red color and lead the shift of absorbance peak to shorter wavelength (Figure S5, Supporting Information). The plasmonic biosensor was optimized with linker concentration (Figure S8, Supporting Information). A clear shift of absorbance peak was observed at linker concentrations of 300 and 400 nM. In contrast, the absorbance peak was not shifted at other linker concentrations. More aggregation at 200 nM linker concentration might happen because insufficient linker concentration did not cause sufficient dispersion of DNA-immobilized GNPs by electric repulsion. On the other hand, more dispersion of 500–700 nM linker concentrations might happen because high linker concentration caused excessive dispersion by electric repulsion. 50 nM detection limit of the plasmonic biosensor was determined by distinguishable color change (Figure 2). This result is comparable to the colorimetric detection of references[24,25] in Table S3, Supporting Information. The specificity of the proposed biosensor could discriminate one base mismatch of the target (Figure 3). Moreover, the proposed colorimetric biosensor showed the possibility of practical use through the detection of a target in the presence of contaminants, and real 16S rRNA target (Figure 4). Therefore, this plasmonic biosensor presents a simple detection method in resource-poor on-site conditions through a combination of DNAzyme amplification and colorimetric GNPs.

4. Conclusion

The proposed plasmonic biosensor could detect *S. choleraesuis* with colorimetric visualization successfully. Multicomponent DNAzyme formed by target addition could cleave the linker effectively at 50 °C. Linker cleavage induced dispersion of two DNA-immobilized GNPs and color change. Under optimized assay conditions, the target could be detected using visual discrimination sensitively and specifically. Moreover, the biosensor showed the possibility of practical use with contaminants and a real 16S rRNA target. As a result, developed plasmonic biosensor could detect a pathogen within 2 h without unstable protein enzyme, specialized technique, or equipment. These advantages could allow that the biosensor would be used for on-site predetection to lower the risk of transmission of infectious diseases.

5. Experimental Section

Materials: Gold(III) chloride trihydrate, sodium citrate tribasic, sodium phosphate dibasic, potassium chloride, and poly(ethylene glycol) methyl ether thiol (M_W = 800 Da) were procured from Sigma-Aldrich, Inc. (St. Louis, Missouri, USA). Magnesium chloride, sodium chloride, and Tris were procured from the Genomic base (Seoul, Korea). Sodium phosphate monobasic and Tween-20 were procured from Generay Biotech (Shanghai, China). Hydrochloric acid and Nitric acid were procured from Duksan pure chemicals (Ansan, Korea). 100 bp Plus DNA Ladder and 6X DNA gel loading buffer 1 (2 Dye) were procured from Biofact (Daejeon, Korea). Nitrocellulose blotting membrane was purchased from GE Healthcare (Buckinghamshire, UK). RNA-containing linker DNA strand and all thiol-modified DNA strands in Table S1, Supporting Information were procured from Integrated DNA Technologies (IDT, Iowa, USA), All other DNA strands were procured from Cosmogenetech, Inc. (Seoul, Korea). DNA strands were resuspended with deionized distilled water (Direct-Pure adept, RephiLe Bioscience) to 100 μM concentration and stored at -20 °C. DNA sequences used in the study are shown in Table S1, Supporting Information. *S. enterica* serotype *choleraesuis* was obtained from ATCC (7001, Manassas, VA, USA). RNeasy Mini Kit was purchased from Qiagen GmbH (Hilden, Germany). RNaseZAP was purchased from Sigma-Aldrich, Inc. (St. Louis, MO, USA).

Instrumentation: The absorbance spectrum was measured from 510 to 540 nm wavelength by microplate spectrophotometer (EPOCH2, Biotek, Vermont, USA). The ultrasonication process was performed using a power sonic 405 (Hwashin instrument, Seoul, Korea). Agarose gel electrophoresis was performed using a Mupid-2 plus (Optima, Japan, Tokyo). The gel image was acquired by the gel documentation system (LSG 1000, iNtRON Biotechnology, Seongnam, South Korea). The diameter of GNPs was measured by DLS (Nano-ZS, Malvern Instruments Ltd., Worcs, UK). SEM images and EDS analysis were acquired using a field emission SEM (JSM-7800F, JEOL Ltd., Tokyo, Japan). TEM images were obtained using a TEM (F200X, Thermo Fisher Scientific, Waltham, MA, USA).

Preparation of 13 nm GNPs: GNPs were synthesized according to the method following a reference.[13] Briefly, 1 mL of 25 nM Gold(III) chloride trihydrate and 98 mL of distilled water were added to a 250 mL Erlenmeyer flask. While the boiling solution was stirred with a magnetic stirrer (HP-3100, Lab companion, Daejeon, Korea), 1 mL of 33 mg mL^{-1} of sodium citrate tribasic was added. After boiling for 10 min, the solution was cooled at room temperature. GNPs were concentrated by centrifugation at 12 000 × *g* for 30 min. Then, Tween-20 was added to a final concentration of 0.01% v/v. Concentration of GNPs was adjusted to 100 nM using 0.01% v/v Tween-20 solution. GNP concentration was calculated based on absorbance at 520 nm measured using a microplate UV–vis spectrophotometer (extinction coefficient of 13 nm GNP: 2.33 × 10^8 M^{-1} cm^{-1}).

Conjugation of Thiolated DNA to GNPs: Thiolated DNA was conjugated to GNPs following a reference's protocol with some modifications.[18] 60 µL of 100 nM 13 nm GNPs and 60 µL of 32 µM one of thiol-modified Imm strand were added to 480 µL of 10 mM phosphate buffer (pH 7.2) with 0.01% v/v Tween-20 in an E-tube. Also, the mixture was incubated for 20 min at room temperature. For stabilization of DNA-conjugated GNPs, 3.43 M NaCl in 10 mM phosphate buffer with 0.01% v/v Tween-20 was added to the mixture solution for ten steps according to the schedule of Table S2, Supporting Information. For each step, the DNA-conjugated GNPs mixture was sonicated for 10 s and incubated for 20 min at room temperature. After the 30 µL addition of 2 mM poly (ethylene glycol) methyl ether thiol (M_W = 800 Da), DNA-conjugated GNPs mixture was incubated for 30 min at 60 °C. Then, DNA-conjugated GNPs were washed three times using centrifugation at 16 000 × *g* for 30 min with 0.01% v/v Tween-20 solution. The final concentration of GNPs was adjusted to 11 nM and stored at 4 °C until use.

Characterization of GNPs: Size, polydispersity, and zeta potential of synthesized GNPs were confirmed using DLS. The GNPs solution was diluted to 1 nM with distilled water. 1 mL of 1 nM GNPs were added to a cuvette (Ratiolab, Dreieich, Germany). After equilibration for 30 s at 25 °C, the size and polydispersity index of GNPs were measured using DLS. Image of synthesized GNPs was acquired using a TEM and EDS analysis. TEM sample was prepared by dropping 1 mL of 1 nM synthesized GNPs on a carbon grid and air-dried overnight. Images and constituent atoms of GNPs, two DNA-conjugated GNPs, and aggregated GNPs were acquired using a SEM and EDS analysis. For each sample, 20 µL aliquot of 0.1 nM was dropped onto an aluminum foil and air-dried overnight and then measured using SEM and EDS.

Colorimetric Detection Using Plasmonic Biosensor: The colorimetric change of GNPs was visually confirmed according to the target concentration. Each tube contains 2 µL of 10× MNAzyme buffer, 2 µL of 150 mM $MgCl_2$, 2 µL of 2 µM MNAzyme subunit A+B solution, 2 µL of 400 nM Linker and 2 µL of 0–1000 nM of the target. The samples were incubated for 1 h at 50 °C in order for the MNAzyme to sufficiently cleave the linker. After the 5 µL addition of 11 nM Imm1-immobilized GNP (GNP-1) and Imm2-immobilized GNP (GNP-2), respectively, the samples were incubated for 20 min at 50 °C and cooled to room temperature for 5 min. Then, 5 µL of the solution was dropped onto the nitrocellulose blotting membrane (8 × 2 cm) at intervals of 1 cm and observed after air-drying overnight. Images were adjusted for contrast and brightness.

Optimized Conditions of Plasmonic Biosensor: To obtain the best performance of the assay, temperature, time, and linker concentration were optimized. For optimization of reaction temperature, each E-tube contains 4 µL of 10× MNAzyme buffer, 4 µL of 150 mM $MgCl_2$, 4 µL of 2 µM MNAzyme subunit A+B solution, 4 µL of 4 µM Linker and 4 µL of 2 µM of the target. Each sample was incubated for 150 min at 50, 55, 60, and 65 °C. For optimization of reaction time, the above samples were incubated at 50 °C for 0, 0.5, 1, 1.5, 2, 3, 4 h. Then, 5 µL of 100 bp DNA ladder and 10 µL of each sample mixed with 6× loading buffer were loaded in a well of 3% agarose gel with 1X TAE buffer. Gel electrophoresis was performed in 1× TAE buffer at a constant potential of 90 V for 15 min using a Mupid-2 plus. The gel image was acquired using the gel documentation system.

For optimization of linker concentration, each tube contains 4 µL of 10× MNAzyme buffer, 4 µL of 150 mM $MgCl_2$, 4 µL of 2 µM MNAzyme subunit A+B solution, 4 µL of 100–700 nM Linker and 4 µL of 0–200 nM of the target. The samples were incubated for 1 h. After 10 µL addition of 11 nM GNP-1 and GNP-2 solutions, the samples were incubated for 20 min at 50 °C and cooled to room temperature for 5 min. Then, the absorbance spectrum of each sample was measured from 510 to 540 nm wavelength using a microplate spectrophotometer. The peak absorbance was plotted according to target concentrations.

Sensitivity and Specificity of the Biosensor: Under optimal conditions, the detection limit was measured under the following conditions. Each 1.7 mL tube containing 4 µL of 10× MNAzyme buffer, 4 µL of 150 mM $MgCl_2$, 4 µL of 2 µM MNAzyme subunit A+B solution, 4 µL of 400 nM Linker and 4 µL of 0–200 nM of the target. After the same procedure above, the absorbance spectrum of each sample was measured between 450 and

600 nm using a microplate spectrophotometer. Mean and standard deviation of peak wavelength was plotted according to the target concentration from triplicate. For the specificity test, M1, M2, and M3 were designed as having one, two, and three adjacent mismatches, respectively (Table S1, Supporting Information). The target was replaced with a mismatched sequence according to 0, 50, 200, and 1000 nm. All the other protocol was the same as the above.

Practical Usability Test of the Biosensor: Practical usability was tested using contaminants and 16S rRNA real targets. First, the Luria–Bertani (LB) broth was used as a contaminant. LB broth was used for the target dilution. The target with LB broth was used for colorimetric detection. Second, the 16S rRNA real target was purified and detected using the biosensor. *S. enterica* serotype Choleraesuis was obtained from ATCC (Manassas, VA, USA) (7001). *S. choleraesuis* strain used in this study was cultured in LB broth at 37 °C and 125 rpm overnight. The number of *Salmonellae* is measured using the plate count technique. The total RNA of *S. choleraesuis* was extracted using the RNeasy Mini Kit was purchased from Qiagen GmbH (Hilden, Germany). The concentration and purity of the extracted total RNA were measured as follows. 2 µL of total RNA was placed in Take3 plates (Biotek Instruments, Inc., Winooski, VT, USA) and measured by microplate spectrophotometer. The diluted total RNA was used as a target and all instruments, and tubes used in the experiment were cleaned using RNaseZap. All the other protocol was the same as the above.

Statistical Analysis: Statistical analyses were performed using a paired *t*-test of the SigmaPlot version 10.0 (Systat Software Inc., San Jose, CA, USA) to assess differences between the two groups.

Supporting Information

Supporting Information is available from the Wiley Online Library or from the author.

Acknowledgements

This research was supported by Basic Science Research Program through the National Research Foundation of Korea (NRF) funded by the Ministry of Science, ICT and Future Planning (NRF-2019R1F1A1063316), by the Marine Biotechnology Program funded by the Ministry of Oceans and Fisheries, Korea.

Conflict of Interest

The authors declare no conflict of interest.

Keywords

diagnosis, DNAzyme, on-site detection, pathogen, plasmonic biosensor

Received: July 30, 2019
Revised: January 6, 2020
Published online: March 4, 2020

[1] R. W. Peeling, D. Mabey, *Clin. Microbiol. Infect.* **2010**, *16*, 1062.
[2] W. G. Lee, Y. G. Kim, B. G. Chung, U. Demirci, A. Khademhosseini, *Adv. Drug Delivery Rev.* **2010**, *62*, 449.
[3] P. Yager, G. J. Domingo, J. Gerdes, *Annu. Rev. Biomed. Eng.* **2008**, *10*, 107.
[4] P. K. Drain, E. P. Hyle, F. Noubary, K. A. Freedberg, D. Wilson, W. R. Bishai, W. Rodriguez, I. V. Bassett, *Lancet Infect. Dis.* **2014**, *14*, 239.
[5] L. M. Abayasekara, J. Perera, V. Chandrasekharan, V. S. Gnanam, N. A. Udunuwara, D. S. Liyanage, N. E. Bulathsinhala, S. Adikary, J. V. S. Aluthmuhandiram, C. S. Thanaseelan, D. P. Tharmakulasingam, T. Karunakaran, J. Ilango, *BMC Infect. Dis.* **2017**, *17*, 631.
[6] H. S. Eom, B. H. Hwang, D. H. Kim, I. B. Lee, Y. H. Kim, H. J. Cha, *Biosens. Bioelectron.* **2007**, *22*, 845.
[7] H. H. Shin, J. H. Seo, C. S. Kim, B. H. Hwang, H. J. Cha, *Biosens. Bioelectron.* **2016**, *79*, 398.
[8] T. S. Hauck, S. Giri, Y. Gao, W. C. Chan, *Adv. Drug Delivery Rev.* **2010**, *62*, 438.
[9] B. H. Hwang, J. W. Lee, H. J. Cha, *Appl. Biochem. Biotechnol.* **2010**, *162*, 1187.
[10] S. Giri, E. A. Sykes, T. L. Jennings, W. C. W. Chan, *ACS Nano* **2011**, *5*, 1580.
[11] K. Hsieh, A. S. Patterson, B. S. Ferguson, K. W. Plaxco, H. T. Soh, *Angew. Chem., Int. Ed.* **2012**, *51*, 4896.
[12] K. Tram, P. Kanda, B. J. Salena, S. Y. Huan, Y. F. Li, *Angew. Chem., Int. Ed.* **2014**, *53*, 12799.
[13] K. Zagorovsky, W. C. Chan, *Angew. Chem., Int. Ed.* **2013**, *52*, 3168.
[14] L. Guo, A. R. Ferhan, H. Chen, C. Li, G. Chen, S. Hong, D. H. Kim, *Small* **2013**, *9*, 234.
[15] L. Guo, Y. Xu, A. R. Ferhan, G. Chen, D. H. Kim, *J. Am. Chem. Soc.* **2013**, *135*, 12338.
[16] L. H. Guo, J. A. Jackman, H. H. Yang, P. Chen, N. J. Cho, D. H. Kim, *Nano Today* **2015**, *10*, 213.
[17] Y. Lin, S. H. Xu, J. Yang, Y. J. Huang, Z. T. Chen, B. Qiu, Z. Y. Lin, G. N. Chen, L. H. Guo, *Sens. Actuators, B* **2018**, *267*, 502.
[18] S. J. Hurst, A. K. R. Lytton-Jean, C. A. Mirkin, *Anal. Chem.* **2006**, *78*, 8313.
[19] J. J. Storhoff, R. Elghanian, R. C. Mucic, C. A. Mirkin, R. L. Letsinger, *J. Am. Chem. Soc.* **1998**, *120*, 1959.
[20] J. Liu, Y. Lu, *J. Fluoresc.* **2004**, *14*, 343.
[21] E. Mokany, S. M. Bone, P. E. Young, T. B. Doan, A. V. Todd, *J. Am. Chem. Soc.* **2010**, *132*, 1051.
[22] K. Schlosser, Y. F. Li, *Chem. Bio. Chem.* **2010**, *11*, 866.
[23] F. Wang, J. Elbaz, C. Teller, I. Willner, *Angew. Chem., Int. Ed.* **2011**, *50*, 295.
[24] C. R. Park, W. J. Rhee, K. W. Kim, B. H. Hwang, *Biotechnol. Bioeng.* **2019**, *116*, 1567.
[25] C. R. Park, S. J. Park, W. G. Lee, B. H. Hwang, *Biotechnol. Bioprocess Eng.* **2018**, *23*, 355.

